International Journal of Non-Linear Mechanics 79 (2016) 26–37

Contents lists available at ScienceDirect

International Journal of Non-Linear Mechanics

journal homepage: www.elsevier.com/locate/nlm

Reconstructing the transient, dissipative dynamics of a bistable Duffing oscillator with an enhanced averaging method and Jacobian elliptic functions

Chunlin Zhang [a,b], R.L. Harne [c,*], Bing Li [a], K.W. Wang [b]

[a] State Key Laboratory for Manufacturing and Systems Engineering, Xi'an Jiaotong University, Xi'an, Shaanxi 710049, PR China
[b] Department of Mechanical Engineering, University of Michigan, Ann Arbor, MI 48109, USA
[c] Department of Mechanical and Aerospace Engineering, The Ohio State University, Columbus, OH 43210, USA

ARTICLE INFO

Article history:
Received 27 March 2015
Received in revised form
4 October 2015
Accepted 4 November 2015
Available online 14 November 2015

Keywords:
Bistable Duffing oscillator
Transient dynamics
Averaging method
Jacobian elliptic functions

ABSTRACT

Systems characterized by the governing equation of the bistable, double-well Duffing oscillator are ever-present throughout the fields of science and engineering. While the prediction of the transient dynamics of these strongly nonlinear oscillators has been a particular research interest, the sufficiently accurate reconstruction of the dissipative behaviors continues to be an unrealized goal. In this study, an enhanced averaging method using Jacobian elliptic functions is presented to faithfully predict the transient, dissipative dynamics of a bistable Duffing oscillator. The analytical approach is uniquely applied to reconstruct the intrawell and interwell dynamic regimes. By relaxing the requirement for small variation of the transient, averaged parameters in the proposed solution formulation, the resulting analytical predictions are in excellent agreement with exact trajectories of displacement and velocity determined via numerical integration of the governing equation. A wide range of system parameters and initial conditions are utilized to assess the accuracy and computational efficiency of the analytical method, and the consistent agreement between numerical and analytical results verifies the robustness of the proposed method. Although the analytical formulations are distinct for the two dynamic regimes, it is found that directly splicing the inter- and intrawell predictions facilitates good agreement with the exact dynamics of the full reconstructed, transient trajectory.

1. Introduction

The governing equation of the bistable, double-well Duffing oscillator has been widely used to evaluate a large variety of nonlinear systems including slender aerostructures that may buckle under loads [1], microelectromechanical switches [2], vibration-based energy harvesters [3,4], electrical circuits [5], and optical systems [6]. Recent developments in smart/adaptive structures have particularly focused on bistable/buckled platforms for performance and functionality enhancements [7], while commercial attention is even lately recognizing the potential for bistability to provide favorable new potentials [8]. The characteristic and strongly nonlinear dynamics of well escape, stochastic resonance, and chaos are uniquely captured by the governing equation of the archetype bistable Duffing oscillator. Together, these features illustrate the broad applicability of the oscillator model in terms of disciplinary relevance as well as for rich, dynamical studies.

Historically, the *transient* dynamics of bistable oscillators have been of great interest, for example as relate to excitations that are impulsive in nature such as blast loading [9], plastic impact [10], and thermal shocks [11], which could induce a critical well escape event or multiple of the "snap-through" behaviors. Based upon the wide applicability of the governing equation of the bistable Duffing oscillator, there is great merit to develop an accurate prediction strategy for the transient, dissipative dynamics of bistable systems.

Using structural terminologies in the study hereafter (e.g., displacement, mass, etc.), the governing equation of the double-well Duffing oscillator and initial conditions examined in this research are expressed using

$$m\ddot{x}+d\dot{x}-k_1x+k_3x^3=0;\quad x(t)|_{t=0}=x_0;\quad \dot{x}(t)|_{t=0}=\dot{x}_0 \tag{1}$$

where m is mass, d is damping constant, k_i $(i=1,3)$ are stiffness constants. Note that while the above expressions and the proposed approach are applicable for all sets of initial conditions $(x_0,\dot{x}_0)$, for the purpose of illustration it is assumed that the oscillator is originally at rest in a statically stable equilibrium with finite initial velocity $\dot{x}(t)|_{t=0}=\dot{x}_0$ throughout this paper. This can be viewed as an example with the system at static equilibrium for $t<0$, and

* Corresponding author.
E-mail address: harne.3@osu.edu (R.L. Harne).

http://dx.doi.org/10.1016/j.ijnonlinmec.2015.11.002
0020-7462/

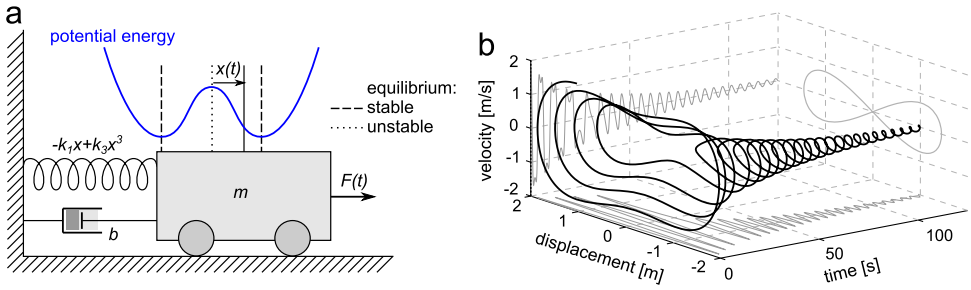

Fig. 1. (a) Schematic of the bistable, double-well Duffing oscillator illustrating the displacement coordinate $x(t)$ convention. (b) Initial velocity imposed on the bistable oscillator originally at rest: interwell vibrations transition into intrawell oscillators as time increases.

under impact loading at $t=0$ such that the velocity immediately changes according to the impulse-momentum theorem. Fig. 1 (a) shows a schematic model of such a bistable oscillator and illustrates the double-well potential energy profile according to the coordinate convention that $x(t)=0$ is the unstable equilibrium when $k_1>0$ and $k_3>0$. In the case where $k_1<0$ and $k_3\neq 0$, Eq. (1) represents the monostable Duffing oscillator which undergoes motions within the individual well of potential energy. In contrast to such behaviors, the bistable oscillator may exhibit two qualitatively distinct dynamics: intrawell oscillations confined to one local well of potential energy and interwell motions which cross the unstable equilibrium. Fig. 1(b) illustrates these distinct dynamic regimes for a bistable oscillator excited with finite initial velocity from a starting position of a stable equilibrium. The dark trajectory in three dimensions is the phase plane of displacement and velocity in time, whereas the projections in displacement–time or velocity–time show the unique contributions in those planes. The (light solid curve) mapping on the far plane of displacement–velocity indicates the homoclinic orbits which differentiate intra- from interwell behaviors according to the instantaneous level of system energy for the undamped oscillator. Due to the amplitude of the imposed initial velocity, interwell dynamics are first activated which lead to approximately 8 crossings between the local wells of potential energy. Then, a period occurs such that the dynamics transition from inter- to intrawell on a time scale sufficiently slower than the natural period of the free oscillations [12]. Finally, the oscillator mass vibrates with small, decaying amplitudes within one of the local wells of potential energy. The accurate analytical prediction of the system response and characterisitics in these two dynamic regimes is the objective of this research.

Numerous methods have been proposed to analytically predict the transient dynamics of the monostable and bistable Duffing oscillator equations. Individual trigonometric functions, specifically sine and cosine, are sometimes assumed to be the analytical solutions [13]. Yet, in practice, such selection leads to poor accuracy when the nonlinearity is considerable [14], $|k_3/k_1|\geq O(1)$, due to the diffusion of energy to many harmonics away from the fundamental [15]. For enhanced accuracy, Barkham and Soudack [16] introduced the Jacobian elliptic functions as generating solutions for the Duffing equation. Since then many approximate analytical solution strategies have been proposed based on the properties of Jacobian elliptic functions. A large variety of such studies have sought to predict the transient dynamics of the monostable Duffing oscillator. Notable contributions have employed these functions in the context of approximate analytical solution strategies including the method of multiple scales [17], the Krylov–Bogoliubov method [18,19], the "C–J" method [20], the averaging method [21], the method of harmonic balance [22], and the homotopy analysis method [23,24].

The Jacobian elliptic functions have also been utilized towards the prediction of the dynamics of bistable Duffing oscillators. Lakrad and Belhaq [25] adopted the multiple scales method to approximate the undamped oscillations. Yuste and Bejarano [14] studied the amplitude decay of a bistable oscillator and reported satisfactory agreement with directly numerically integrated results for small degrees of nonlinearity. Yuste [26] extended the harmonic balance method to enable the approximation of several cycles of oscillation when the nonlinearity was non-trivial. Cveticanin [27] approximated the transient behaviors using complex generating functions and demonstrated two examples that showed good agreement with numerical results. These advancements have provided new pathways towards the prediction of the transient behaviors of bistable Duffing oscillators. On the other hand, by their implementation of the Jacobian elliptic functions having fixed modulus/phase, the approximations are suitable for only a few cycles of dissipative oscillation and may be severely limited in parameter selection for favorable results.

The objective of this research is to develop an enhanced analytical prediction strategy for the transient dynamics of bistable oscillators. The aim is to faithfully reconstruct the motions over a large number of free decay vibration cycles including both intra- and interwell behaviors, and with high-fidelity for a significant range of system parameters. A promising idea to meet this goal is to leverage the averaging method with the Jacobian elliptic functions. Indeed, Coppola and Rand [28,29] employed these tools to approximate the transient dynamics of several monostable, nonlinear oscillators, which was the strategy likewise followed by Belhaq and Lakrad [30]. However, the classical averaging method is based upon a near-identity transformation [15] which assumes that the time rate of change of the averaged amplitude of oscillation is sufficiently small [28]. As a result, the applicability of the classical method is limited to generating accurate predictions for the case of small oscillations near equilibria. Yet, when considering bistable Duffing oscillators, the interwell vibrations are characteristically "far from equilibrium" and therefore undergo large amplitude decay from initial conditions, prior to transitioning to intrawell behaviors which eventually become near-linear motions. It is clear that the classical averaging method is unsuitable to predict such a significant variation in dynamics.

To advance the state of the art and overcome these limitations for an accurate and long-time prediction of the transient dynamics of bistable oscillators, this research develops an enhanced averaging method with the Jacobian elliptic functions building upon the method established by Coppola and Rand [28]. Yet, instead of applying near-identity transformations that limit applicability to oscillations near equilibria, the approach developed here enables slow variation in oscillation amplitude and modulus/phase so that the full dynamic range of motions of the bistable system may be accurately reconstructed. The following sections detail this new strategy as individually applied to the intrawell and interwell oscillations regimes. Because previous endeavors have only succeeded in reconstructing a few of the transient oscillation cycles of bistable oscillators or the overall amplitude decay [31], the most

constructive and comprehensive assessments of the developments in this research are obtained by comparison of the current analytical predictions to results of numerically integrating the governing equations, considered to be the exact dynamics. Such a rigorous assessment is then presented, exploring the accuracy of the proposed approach using a large range of system and excitation parameters. Prior to concluding remarks, a discussion is provided to summarize and examine the applicability, limitations, and potential of the proposed analytical approach.

2. Analytical prediction formulations for the undamped system: intra- and interwell oscillations

The schematic model illustrated in Fig. 1(a) is analyzed here. From Eq. (1), by setting

$$\gamma = d/m, \quad \alpha = k_1/m, \quad \beta = k_3/m, \tag{2}$$

the governing equation is simplified as

$$\ddot{x}+\gamma\dot{x}-\alpha x+\beta x^3=0; \quad x|_{t=0}=x_0; \quad \dot{x}|_{t=0}. \tag{3}$$

Eq. (3) is used throughout the remainder of this research. Note that the fixed points (equilibria) of the system occur at $x^*=\left\{0, \pm\sqrt{\alpha/\beta}\right\}$, where the unstable equilibrium is $x^*=0$ and the latter two, non-zero values are stable equilibria. Additionally, note that the total energy of the system is $E(t)=\left(2\dot{x}^2-2\alpha x^2+\beta x^4\right)/4$, so that the homoclinic orbits (here at $E=0$) are defined by $\dot{x}=\pm\sqrt{\alpha x^2-\beta x^4/2}$. Therefore, intrawell behaviors satisfy $E<0$ whereas interwell oscillations occur when $E>0$.

In the absence of damping $(\gamma=0)$

$$\ddot{x}-\alpha x+\beta x^3=0, \quad x|_{t=0}=x_0, \quad \dot{x}|_{t=0}=\dot{x}_0. \tag{4}$$

Researchers have shown that the equation of motion for the undamped, bistable Duffing oscillator is exactly solved using Jacobian elliptic functions [15,32]. In the following, x_d represents the intrawell vibration and x_c denotes the interwell vibration.

For intrawell vibration, the response is obtained by assuming the solution of Eq. (4) in the form [32]

$$x_d=\zeta D_0 dn(\omega_d t+\varphi_{d0}, k_d)=\zeta D_0 dn(u_d, k_d)\equiv\zeta D_0 dn \tag{5}$$

where $\zeta=\pm1$ is defined in Eq. (8); u_d and k_d are the argument and modulus of Jacobian elliptic function $dn(u_d, k_d)$, respectively [33]. The period of $dn(u_d, k_d)$ is $2K(k_d)$, where $K(k_d)$ is the complete elliptic integral of the first kind and is hereafter expressed as K_d for brevity. In the absence of damping, ω_d and k_d are constants, and φ_{d0} is the initial argument and is determined by initial conditions. By taking the derivatives of Eq. (5) and substituting appropriate relations into (4), one finds that

$$\omega_d^2=\beta D_0^2/2; \quad k_d^2=2-2\alpha/\left(\beta D_0^2\right). \tag{6}$$

Thus, the undamped, intrawell oscillations are described using

$$x_d=\zeta D_0 dn\left(\sqrt{\beta D_0^2/2}\cdot t+\varphi_{d0}, \left[2-2\alpha/\left(\beta D_0^2\right)\right]^{1/2}\right). \tag{7}$$

In Eq. (7), the sign indicator ζ, initial amplitude D_0, and initial argument φ_{d0} are all determined by the initial conditions. ζ indicates the intrawell position and is expressed as

$$\zeta=\begin{cases} sgn[x_0], & \text{if } x_0\neq0 \\ sgn[\dot{x}_0], & \text{if } x_0=0 \end{cases}. \tag{8}$$

The initial displacement and velocity when $t=0$ satisfy

$$x_0=\zeta D_0 dn(\varphi_{d0}, k_d); \quad \dot{x}_0=-\zeta D_0\omega_d k_d^2 sn(\varphi_{d0}, k_d)cn(\varphi_{d0}, k_d). \tag{9}$$

Using the identities of the Jacobian elliptic functions [33], the initial amplitude and phase are found to be

$$D_0=\beta^{-1/2}\cdot\left(\alpha+\sqrt{(\alpha-\beta x_0^2)^2+2\beta\dot{x}_0^2}\right)^{1/2}; \quad \frac{sn(\varphi_{d0}, k_d)cn(\varphi_{d0}, k_d)}{dn(\varphi_{d0}, k_d)}$$

$$=-\frac{\dot{x}_0}{x_0\omega_d k_d^2}. \tag{10}$$

When the initial energy of the bistable oscillator is sufficient to induce interwell vibration ($E|_{t=0}>0$), the exact vibration response can be found by assuming the solution of Eq. (4) in the following form [15]

$$x_c=C_0 cn(\omega_c t+\varphi_{c0}, k_c)=C_0 cn(u_c, k_c)\equiv C_0 cn \tag{11}$$

where u_c and k_c are the argument and modulus of the Jacobian elliptic function $cn(u_c, k_c)$, respectively. The period of $cn(u_c, k_c)$ is $4K(k_c)$, where $K(k_c)$ is the complete elliptic integral of the first kind with respect to the modulus of k_c and is hereafter expressed as K_c for brevity. When damping is absent, ω_c and k_c are constants, and φ_{c0} is the initial argument which is determined by initial conditions. Likewise, by taking the derivatives of Eq. (11) and substituting appropriate relations into (4), one finds that

$$\omega_c^2=\beta C_0^2-\alpha; \quad k_c^2=\beta C_0^2/(2\omega_c^2)=\beta C_0^2/\left[2(\beta C_0^2-\alpha)\right]. \tag{12}$$

Thus, the unperturbed interwell vibration of Eq. (4) is expressed by

$$x_c=C_0 cn\left(\sqrt{\beta C_0^2-\alpha}\cdot t+\varphi_{c0}, \left(\frac{\beta C_0^2}{2(\beta C_0^2-\alpha)}\right)^{1/2}\right). \tag{13}$$

From Eq. (13), the argument u_c and modulus k_c are functions of the amplitude C_0. Here, the initial amplitude C_0 and argument φ_{c0} depend on initial conditions:

$$x_0=C_0 cn(\varphi_{c0}, k_c); \quad \dot{x}_0=-\omega_c C_0 sn(\varphi_{c0}, k_c)\cdot dn(\varphi_{c0}, k_c) \tag{14}$$

Using the elliptic function identities [33], the initial amplitude and phase are found

$$C_0=\beta^{-1/2}\cdot\left(\alpha+\sqrt{(\alpha-\beta x_0^2)^2+2\beta\dot{x}_0^2}\right)^{1/2}; \quad \frac{sn(\varphi_{c0}, k_c)}{cn(\varphi_{c0}, k_c)}\cdot dn(\varphi_{c0}, k_c)$$

$$=-\frac{\dot{x}_0}{\omega_c x_0}. \tag{15}$$

2.1. Constraints on the parameters

For the Jacobian elliptic functions $sn(u,k)$, $cn(u,k)$ and $dn(u,k)$, the modulus is intrinsically constrained to satisfy $0\le k^2\le1$. By applying this constraint to the analytical solution of intrawell vibration, one finds

$$0\le k_d^2\le1 \quad\Leftrightarrow\quad 1/2\le \alpha/\left(\beta D_0^2\right)\le1. \tag{16}$$

Considering the instantaneous displacement and velocity of intrawell vibration are $x_d=\zeta D_0 dn$ and $\dot{x}_d=-\zeta D_0\omega_d k_d^2 sncn$, respectively, the instantaneous system energy then can be derived as

$$E_d=\dot{x}_d^2/2-\alpha x_d^2/2+\beta x_d^4/4=D_0^2\left(\beta D_0^2-2\alpha\right)/4. \tag{17}$$

According to Eqs. (16) and (17), when the instantaneous energy is negative, the bistable oscillator undergoes intrawell oscillations which are expressible using $dn(u_d, k_d)$. On the other hand, for interwell vibration, application of the above modulus constraint leads to

$$0\le k_d^2\le1 \quad\Leftrightarrow\quad 0\le\alpha/\left(\beta C_0^2\right)\le1/2. \tag{18}$$

Considering that the displacement and velocity are expressed using $x_c = C_0 cn$ and $\dot{x}_c = -C_0\omega_c sndn$, the instantaneous energy is

$$E_c = \dot{x}_c^2/2 - \alpha x_c^2/2 + \beta x_c^4/4 = C_0^2\left(\beta C_0^2 - 2\alpha\right)/4. \tag{19}$$

Similarly, when the energy is positive, the bistable oscillator undergoes interwell vibration such that the undamped dynamics are described by $cn(u,k)$. Therefore, $\beta A^2 = 2\alpha$ is the critical condition demarcating the intra- from the interwell oscillation regimes, in which A is the amplitude corresponding to D_0 and C_0, respectively.

3. Approximate prediction of the damped, intrawell vibration

The intrawell vibration of the damped bistable oscillator, $\gamma > 0$, is assumed to satisfy the form in Eq. (5) while the amplitude $D = D(t)$ and argument $u_d = 2K_d\psi_d(t)$ both slowly vary in time. The new variable $2K_d\psi_d$ is used as the argument because it leads to periodically variational equations that can be averaged. The other variables are amplitude dependent and satisfy Eq. (6) from the undamped relations.

$$x_d(t) = \zeta D(t) dn\left(2K_d\psi_d, k_d\right) = \zeta D(t) dn(u_d, k_d) \equiv \zeta D dn \tag{20a}$$

$$\dot{x}_d = \zeta D\omega_d dn' \tag{20b}$$

$$K_d = K(k_d),\quad k_d^2 = 2 - 2\alpha/\beta D^2,\quad \omega_d^2 = \beta D^2/2. \tag{20c}$$

Differentiating Eq. (20a), one obtains the first-order derivative of x_d as

$$\dot{x}_d = \zeta\frac{dD}{dt}\left[dn + 2D\psi_d K_d' k_d' dn' + Dk_d'\frac{\partial dn}{\partial k_d}\right] + \zeta\frac{d\psi_d}{dt}2DK_d dn' \tag{21}$$

where $(\cdot)'$ denotes differentiation of the variable with respect to its argument, thus

$$K_d' \equiv \frac{dK_d}{dk_d},\quad k_d' \equiv \frac{dk_d}{dD},\quad \omega_d' \equiv \frac{d\omega_d}{dD},\quad dn' \equiv \frac{\partial dn(u_d, k_d)}{\partial u_d}. \tag{22}$$

Comparing Eqs. (20b) and (21) one finds

$$\frac{dD}{dt}\left[dn + 2D\psi_d K_d' k_d' dn' + Dk_d'\frac{\partial dn}{\partial k_d}\right] + \frac{d\psi_d}{dt}\cdot 2DK_d dn' = D\omega_d dn'. \tag{23}$$

From Eq. (20b), the second-order derivative of x_d can be derived as

$$\ddot{x}_d = \zeta\left\{\frac{dD}{dt}\left[\left(\omega_d + D\omega_d'\right)dn' + 2D\psi_d\omega_d K_d' k_d' dn'' + D\omega_d k_d'\frac{\partial dn'}{\partial k_d}\right] + \frac{d\psi_d}{dt}\cdot 2DK_d\omega_d dn''\right\}. \tag{24}$$

Substituting Eqs. (20) and (24) into (3), one obtains

$$\frac{dD}{dt}\left[\left(\omega_d + D\omega_d'\right)dn' + 2D\psi_d\omega_d K_d' k_d' dn'' + D\omega_d k_d'\frac{\partial dn'}{\partial k_d}\right] + \frac{d\psi_d}{dt}\cdot 2DK_d\omega_d dn'' + \gamma D\omega_d dn' - \alpha D dn + \beta D^3 dn^3 = 0. \tag{25}$$

Combining Eqs. (23) and (25), dD/dt and $d\psi_d/dt$ are solved to yield

$$\frac{dD}{dt} = -\frac{\gamma D}{k_d^2}dn'^2 = -\frac{\gamma D}{k_d^2}\left[k_d^2 - 1 + \left(2 - k_d^2\right)dn^2 - dn^4\right] \tag{26a}$$

$$\frac{d\psi_d}{dt} = \frac{\omega_d}{2K_d} + \frac{\gamma dn'}{2K_d k_d^2}\left\{dn - \frac{2 - k_d^2}{k_d^2\left(1 - k_d^2\right)}\left[Z(u_d, k_d)dn' + dn\left(1 - dn^2\right)\right]\right\} \tag{26b}$$

where $Z(u_d, k_d)$ is the Jacobian Zeta function. Eq. (26) is non-integrable so that here the averaging method is utilized to obtain analytical approximations of the amplitude D and phase ψ_d.

3.1. Approximation of the decaying amplitude D for intrawell vibration

The oscillation amplitude smoothly decreases as time proceeds and is assumed to be nearly constant over one period of the vibration (i.e., a period of $2K_d$ with respect to argument u_d). Thus, parameters k_d^2, ω_d, and K_d which are functions of the amplitude D are also considered to remain nearly constant over one period. Consequently, instead of being assumed sufficiently small as in the classical averaging method, by Eq. (26) the variables $\dot{D}$ and $\dot{\psi}_d$ are assumed to slowly vary by a finite degree due to the relation to the Jacobian elliptic functions. Therefore, the averaged variables over one period $2K_d$ are smooth, local means of the instantaneous variables and are thus termed "averaged instantaneous variables". The averaged instantaneous amplitude is derived from Eq. (26a) to yield

$$\begin{aligned}\dot{\overline{D}} &= -\frac{\gamma\overline{D}\left(k_d^2 - 1\right)}{k_d^2} - \frac{\gamma\overline{D}\left(2 - k_d^2\right)}{k_d^2}\cdot\frac{1}{2K_d}\int_0^{2K_d} dn^2 du_d \\ &\quad + \frac{\gamma\overline{D}}{k_d^2}\cdot\frac{1}{2K_d}\int_0^{2K_d} dn^4 du_d \\ &= -\gamma\overline{D}\left[\frac{2\left(k_d^2 - 1\right)}{3k_d^2} + \frac{2 - k_d^2}{3k_d^2}\cdot\frac{E_d}{K_d}\right] \Rightarrow \dot{D} = -\gamma D\left[\frac{2\left(k_d^2 - 1\right)}{3k_d^2} + \frac{2 - k_d^2}{3k_d^2}\cdot\frac{E_d}{K_d}\right]\end{aligned} \tag{27}$$

where K_d and E_d denote the complete elliptic integrals of the first and second kinds, respectively; and $\overline{D}$ is very close to D and so that $\overline{D}$ is replaced by D since the latter is nearly constant over one period of oscillation. Eq. (27) is non-integrable and the right side is an implicit function of D. To find an explicit and integrable approximation of Eq. (27), a polynomial fit is employed. Eq. (27) is rewritten as

$$\dot{D} = -\gamma D\cdot f(k_d^2);\quad f\left(k_d^2\right) = \frac{2\left(k_d^2 - 1\right)}{3k_d^2} + \frac{2 - k_d^2}{3k_d^2}\cdot\frac{E_d}{K_d}. \tag{28}$$

Considering the values of elliptic integrals E_d and K_d are completely determined by k_d^2, thus $f\left(k_d^2\right)$ is a pure function depending on k_d^2. Recalling Eqs. (6) and (16), the mapping correspondence $\alpha/\beta D^2 \to k_d^2$ is a bijection. Thus $f\left(k_d^2\right)$ could also be expressed as a function of $\alpha/\beta D^2$ by changing the independent variable from k_d^2 to $\alpha/\beta D^2$. The values of k_d^2 and $f\left(k_d^2\right)$ are calculated sequentially on the range of $1/2 \le \alpha/\beta D^2 \le 1$ by using Eqs. (6) and (28), respectively. Accordingly, the mapping correspondence of $\alpha/\beta D^2 \to f\left(k_d^2\right)$ is numerically established to enable the analytical integration of Eq. (27).

It is found that $f\left(k_d^2\right)$ is smooth on a large range of $0.55 \le \alpha/\beta D^2 \le 1$ and is sufficiently approximated via an individual polynomial fit using

$$f\left(k_d^2\right) \approx p_1 = \mu\cdot\left(\frac{\alpha}{\beta D^2}\right)^{\lambda} + \upsilon. \tag{29}$$

where μ, υ, and λ are undetermined coefficients. A beneficial advantage of Eq. (29) is that it provides an integrable approximation of Eq. (27). For different values of λ, μ and υ are calculated using a linear fit. The performance of various fitting parameter sets is estimated using $R^2 = 1 - SSE/SST$, where SSE is the sum of squared residuals and SST is the sum of squared $f\left(k_d^2\right)$, so that

higher values of R^2 indicate improvements in the fitting to the exact $f\left(k_d^2\right)$. By this procedure, a high-fidelity fit of $R^2=0.9987$ is realized across $0.55\le\alpha/\beta D^2\le 1$ using $\lambda=2$, $\mu=-0.15011$, and $\upsilon=0.14714$. By substituting Eq. (29) into (28) and integrating the result, the decaying amplitude of intrawell oscillation is found

$$D=\left[\left(\frac{\mu}{\upsilon}\alpha^2+\beta^2D_0^4\right)e^{-4\upsilon\gamma t}-\frac{\mu}{\upsilon}\alpha^2\right]^{1/4}\cdot\beta^{-1/2} \tag{30}$$

where D_0 is the initial amplitude determined by initial conditions, expressed in Eq. (10). Thus, the velocity amplitude of the oscillation is given by Eq. (20b) according to the displacement amplitude D.

3.2. Time trajectories of intrawell displacement

The instantaneous displacement is expressed in Eq. (20a). To reconstruct the trajectory in time, the unknown argument $u_d=2K_d\psi_d$ of the Jacobian elliptic function $dn(u_d,k_d)$ must be approximated. The first order derivative of $2K_d\psi_d$ is

$$\dot{u}_d=\frac{d}{dt}(2K_d\psi_d)=2\psi_d\frac{dK_d}{dk_d}\frac{dk_d}{dD}\frac{dD}{dt}+2K_d\frac{d\psi_d}{dt}=2\psi_dK_d'k_d'\dot{D}+2K_d\dot{\psi}_d. \tag{31}$$

Then, K_d' and k_d' are expressed by

$$K_d'\equiv\frac{dK_d}{dk_d}=\frac{1}{k_d}\left(\frac{E_d}{l_d^2}-K_d\right);\quad k_d'\equiv\frac{dk_d}{dD}=\frac{1}{k_d}\frac{2\alpha}{\beta D^3}=\frac{2-k_d^2}{k_d}\cdot\frac{1}{D}. \tag{32}$$

Substituting Eqs. (27) and (32) into (31) and averaging the result, one obtains

$$\dot{\bar{u}}=-2\gamma\psi_d\frac{2-k_d^2}{k_d^2}\left(\frac{E_d}{l_d^2}-K_d\right)\left(\frac{2\left(k_d^2-1\right)}{3k_d^2}+\frac{2-k_d^2}{3k_d^2}\frac{E_d}{K_d}\right)+\omega_d. \tag{33}$$

Note that ψ_d and u_d depend on the intrawell oscillation amplitude D and thus they slowly vary during one period $2K_d$. Accordingly, ψ_d and u_d are approximated by the averaged instantaneous parameters $\bar{\psi}_d$ and $\bar{u}_d$, and from Eq. (5) the initial values of ψ_d and u_d are $\varphi_{d0}/2K_d$ and φ_{d0}, respectively. By averaging over one period $[0,\ 2K_d]$, it is found that $\bar{\psi}_d=\omega_d/2K_d$. Thus, ψ_d and u_d can be approximated as

$$\psi_d(t)=\psi_d(0)+\int_0^t\dot{\psi}_d dt\cong\frac{\varphi_{d0}}{2K_d}+\int_0^t\dot{\bar{\psi}}_d dt=\frac{\varphi_{d0}}{2K_d}+\int_0^t\frac{\omega_d}{2K_d}dt \tag{34a}$$

$$u_d(t)=u_d(0)+\int_0^t\dot{u}_d dt\cong\varphi_{d0}+\int_0^t\left\{-2\gamma\psi_d\frac{2-k_d^2}{k_d^2}\left(\frac{E_d}{l_d^2}-K_d\right)\left(\frac{2\left(k_d^2-1\right)}{3k_d^2}+\frac{2-k_d^2}{3k_d^2}\frac{E_d}{K_d}\right)+\omega_d\right\}dt \tag{34b}$$

in which φ_{d0} is the initial argument determined by initial conditions in Eq. (10) which is readily calculated using the Jacobian inverse elliptic functions. Though the integration of Eq. (34) is not possible analytically, the integrand contains only functions of the amplitude and thus the integration may be numerically determined. As a result, in this study ψ_d and u_d are calculated using trapezoidal integration based upon the analytically-derived amplitude following the approach developed in Section 3.1.

4. Approximate prediction of the damped, interwell vibration

The bistable oscillator undergoes interwell vibration when the transient system energy is positive, $E(t)>0$. Using a similar strategy as that employed for the intrawell vibrations in Section 3, the analytical prediction of the transient, dissipative interwell dynamics is developed for the bistable oscillator. The interwell vibration of the damped system in Eq. (3) is assumed to satisfy the solution form in Eqs. (11) and (12) while parameters $C=C(t)$ and $\psi_c=\psi_c(t)$ are assumed to slowly vary in time. The variable $4K_c\psi_c$ is used as the argument. Then,

$$x_c=C(t)cn(u_c,k_c)=C(t)cn(4K_c\psi_c,k_c)\equiv Ccn \tag{35a}$$

$$\dot{x}_c=C\omega_c cn' \tag{35b}$$

$$K_c=K(k_c),\ \ k_c^2=\beta C^2/(2\omega_c^2),\ \ \omega_c^2=\beta C^2-\alpha. \tag{35c}$$

The velocity $\dot{x}_c$ is also obtained by differentiating Eq. (35a)

$$\dot{x}_c=\frac{dC}{dt}\left[cn+4C\psi_cK_c'k_c'cn'+Ck_c'\frac{\partial cn}{\partial k_c}\right]+\frac{d\psi_c}{dt}\cdot 4CK_ccn' \tag{36}$$

and

$$K_c'\equiv dK_c/dk_c,\ \ k_c'\equiv dk_c/dC,\ \ \omega_c'\equiv d\omega_c/dC,\ \ cn'\equiv\partial cn(u_c,k_c)/\partial u_c. \tag{37}$$

Comparing Eqs. (35b) and (36) leads to

$$\frac{dC}{dt}\left[cn+4C\psi_cK_c'k_c'cn'+Ck_c'\frac{\partial cn}{\partial k_c}\right]+\frac{d\psi_c}{dt}\cdot 4CK_ccn'=C\omega_ccn'. \tag{38}$$

From Eq. (35b), the second order derivative of x_c is derived as

$$\ddot{x}_c=\frac{dC}{dt}\left[(\omega_c+C\omega_c')cn'+4C\psi_c\omega_cK_c'k_c'cn''+C\omega_ck_c'\frac{\partial cn'}{\partial k_c}\right]+\frac{d\psi_c}{dt}\cdot 4CK_c\omega_ccn''. \tag{39}$$

Substituting Eqs. (35) and (39) into Eq. (3) one obtains

$$\frac{dC}{dt}\left[(\omega_c+C\omega_c')cn'+4C\psi_c\omega_cK_c'k_c'cn''+C\omega_ck_c'\frac{\partial cn'}{\partial k_c}\right]+\frac{d\psi_c}{dt}\cdot 4CK_c\omega_ccn''+\gamma C\omega_ccn'-\alpha Ccn+\beta C^3cn^3=0. \tag{40}$$

Combining Eqs. (38) and (40), dC/dt and $d\psi_c/dt$ are found

$$dC/dt=-\gamma C(cn')^2 \tag{41a}$$

$$d\psi_c/dt=\left\{\omega_c+\gamma cn'\left[cn-\left(1-2k_c^2\right)\left(Z(u_c,k_c)cn'+k_c^2cn\left(1-cn^2\right)\right)/\left(1-k_c^2\right)\right]\right\}/4K_c \tag{41b}$$

where $Z(u,k)$ is the Jacobian Zeta function and Z_c is the notation used here to indicate $Z(u_c,k_c)$. Like before, Eq. (41) is not able to be integrated analytically so a similar strategy of averaging and polynomial fitting is employed to develop approximate predictions for the averaged instantaneous interwell vibration amplitude and argument.

4.1. Approximation of the decaying amplitude C for interwell vibration

The averaged instantaneous amplitude of oscillation is obtained using the averaging method over one period $[0,4K_c]$.

$$\dot{\bar{C}}=-\gamma\bar{C}\frac{1}{4K_c}\int_0^{4K_c}cn'^2(u_c,k_c)du_c=-\frac{\gamma\bar{C}}{4K_c}\left[\int_0^{4K_c}sn^2du_c-\int_0^{4K_c}k_c^2sn^4du_c\right]$$
$$=-\gamma\bar{C}\left[\frac{1-k_c^2}{3k_c^2}+\frac{2k_c^2-1}{3k_c^2}\frac{E_c}{K_c}\right]\Rightarrow\dot{C}=-\gamma C\left[\frac{1-k_c^2}{3k_c^2}+\frac{2k_c^2-1}{3k_c^2}\frac{E_c}{K_c}\right] \tag{42}$$

where $E_c=E(k_c)$ and $K_c=K(k_c)$ are the complete elliptic integral of the second and first kinds, respectively; and the averaged instantaneous amplitude $\bar{C}$ is smooth local mean of the vibration

amplitude C. Considering that $\overline{C}$ is very close to C, $\overline{C}$ is therefore replaced by C in Eq. (42). The right side of Eq. (42) is an implicit function of the amplitude C. To enable a polynomial fitting procedure for the right-hand side of Eq. (42), the equation may be written

$$\dot{C} = -\gamma C \cdot h\left(k_c^2\right); \quad h\left(k_c^2\right) = \frac{1-k_c^2}{3k_c^2} + \frac{2k_c^2-1}{3k_c^2}\frac{E_c}{K_c}. \tag{43}$$

Note that the complete elliptic integrals E_c and K_c are determined by k_c^2, and $h\left(k_c^2\right)$ is a function that depends on argument k_c^2. Recalling Eqs. (18) and (35c), it is evident that the mapping correspondence $\alpha/\beta C^2 \to k_c^2$ is a bijection. Thus, one may change the argument from k_c^2 to $\alpha/\beta C^2$, and $h\left(k_c^2\right)$ could be expressed as a function of $\alpha/\beta C^2$. On the range of $0 \le \alpha/\beta C^2 \le 0.5$, the values of k_c^2 and $h\left(k_c^2\right)$ are calculated sequentially by Eqs. (35c) and (43), respectively. Accordingly, the mapping correspondence $\alpha/\beta C^2 \to h\left(k_c^2\right)$ is numerically established to enable the analytical integration of Eq. (42).

It is found that $h\left(k_c^2\right)$ is sufficiently approximated by an individual polynomial fit across the broad range of $0.05 \le \alpha/\beta C^2 \le 0.45$ using

$$h\left(k_c^2\right) \approx q_1 = a \cdot \left(\frac{\alpha}{\beta C^2}\right)^n + b \tag{44}$$

where a, b, and n are undetermined coefficients. Using linear polynomial fitting,a and b are determined for a range of selections of n where the best fitting performance is obtained at $R^2 = 0.9962$ when $n = 2$, $a = -0.78592$, and $b = 0.32051$. By substituting Eq. (44) into (42) and integrating the result, the amplitude of interwell oscillation is found to be

$$C(t) = \left[\left(\beta^2 C_0^4 + \frac{a}{b}\alpha^2\right)e^{-4b\gamma t} - \frac{a}{b}\alpha^2\right]^{1/4} \cdot \beta^{-1/2} \tag{45}$$

where C_0 is the initial amplitude determined by initial conditions, Eq. (15). By Eq. (35b), the velocity amplitude is calculated from the decaying amplitude of displacement. Considering the criteria which demarcates intra- from interwell oscillations, $\beta A^2 = 2\alpha$, the time at which the analytical prediction estimates the interwell oscillations to cease is given by

$$t_{end} = -\ln\left[(4+a/b)\alpha^2 \cdot \left(\beta^2 C_0^4 + \alpha^2 a/b\right)^{-1}\right]/4b\gamma. \tag{46}$$

4.2. Time trajectories of interwell displacement

The instantaneous interwell displacement is expressed in Eq. (35a). Prior to its determination, the argument $u_c = 4K_c\psi_c$ of the Jacobian elliptic function $cn(u_c, k_c)$ must be estimated. The first order derivative of the argument is obtained as

$$\dot{u}_c \equiv \frac{du_c}{dt} = \frac{d}{dt}(4K_c\psi_c) = 4\psi_c\frac{dK_c}{dk_c}\frac{dk_c}{dC}\frac{dC}{dt} + 4K_c\frac{d\psi_c}{dt} = 4\psi_c K_c' k_c' \dot{C} + 4K_c\dot{\psi}_c. \tag{47}$$

Then, K_c' and k_c' are expressed by

$$K_c' \equiv \frac{dK_c}{dk_c} = \frac{K_c}{k_c l_c^2}\left(\frac{E_c}{K_c} - l_c^2\right) = \frac{1}{k_c}\left(\frac{E_c}{l_c^2} - K_c\right);$$
$$k_c' \equiv \frac{dk_c}{dC} = -\frac{\beta C\alpha}{\left(\beta C^2 - \alpha\right)^2}\frac{1}{2k_c} = -\left(2k_c^2 - 1\right)\frac{k_c}{C}. \tag{48}$$

Substituting Eq. (48) into (47) and averaging the result, one obtains

$$\dot{\overline{u}}_c = 4\gamma\psi_c\left(\frac{E_c}{l_c^2} - K_c\right)\left(2k_c^2 - 1\right)\left[a\left(\frac{\alpha}{\beta C^2}\right)^2 + b\right] + \omega_c. \tag{49}$$

Considering that ψ_c and u_c are functions of the interwell vibration amplitude and thus also slowly vary during one period $4K_c$, ψ_c and u_c can be approximated by the averaged instantaneous parameters $\overline{\psi}_c$ and $\overline{u}_c$, having initial values ψ_c and u_c are $\varphi_{c0}/4K_c$ and φ_{c0}, respectively, from Eq. (11). By averaging over one period $[0,\ 4K_c]$, it is found that $\dot{\overline{\psi}}_c = \omega_c/4K_c$. Thus ψ_c and u_c are approximated by

$$\psi_c(t) = \psi_c(0) + \int_0^t \dot{\psi}_c dt \cong \frac{\varphi_{c0}}{4K_c} + \int_0^t \dot{\overline{\psi}}_c dt = \frac{\varphi_{c0}}{4K_c} + \int_0^t \frac{\omega_c}{4K_c} dt \tag{50a}$$

$$u_c(t) = u_c(0) + \int_0^t \dot{u}_c dt \cong \varphi_{c0} + \int_0^t \left\{4\gamma\psi_c\left(\frac{E_c}{l_c^2} - K_c\right)\left(2k_c^2 - 1\right) \times \left[a\left(\frac{\alpha}{\beta C^2}\right)^2 + b\right] + \omega_c\right\} dt \tag{50b}$$

in which, φ_{c0} is the initial argument determined by the amplitude and velocity and is calculated via the Jacobian inverse elliptic functions. Though the integration of Eq. (50) is not possible analytically, the integrand contains only functions of the amplitude and may be determined numerically. Thus, as for intrawell oscillations, the interwell argument u_c is determined numerically by trapezoidal integration from the analytically-derived amplitude $C(t)$, after which the instantaneous displacement $x_c(t)$ is found by Eq. (35).

5. Accuracy of the analytical predictions

This section assesses the accuracy of the proposed analytical solution strategy towards predicting the transient, dissipative dynamics of the bistable oscillator. The prediction capabilities for intra- and interwell dynamics are individually evaluated. For consistency throughout, the value of linear stiffness is $\alpha = 1$ and the initial displacement is the stable equilibrium $x_0 = +\sqrt{\alpha/\beta}$. Thus, to initiate the dynamics away from equilibrium, a variety of initial velocities are imposed, which, by the constraints described in Section 2.1, accordingly induce either intra- or interwell oscillations. The exact transient dynamics are presumed to be those solutions obtained by direct numerical integration of the governing Eq. (3) with a fourth-order Runge–Kutta algorithm conducted in the software MATLAB where the relative integration tolerance is set to be three orders of magnitude more refined than the default tolerance (further refined tolerances did not affect results). In addition to several examples providing qualitative comparisons between time/velocity trajectories as predicted by the analysis and by numerical integration, a quantitative evaluation of the analytical prediction accuracy is achieved by computing the correlation coefficient $\rho_{a,n} \equiv \mathrm{cov}(x_a, x_n) \cdot [\mathrm{cov}(x_a, x_a) \cdot \mathrm{cov}(x_n, x_n)]^{-1/2} \in [0, 1]$ between the analytical x_a and numerical x_n displacement results. This measure has the merit that it simultaneously evaluates the accuracy of both amplitude and phase properties of the trajectories.

5.1. Transient intrawell oscillations

For initial qualitative assessments of the analysis against the numerical computations, the dynamics of a bistable oscillator having parameters $\gamma = 0.034427$ and $\beta = 0.98237$ are considered in the regime in which initial conditions lead to only intrawell

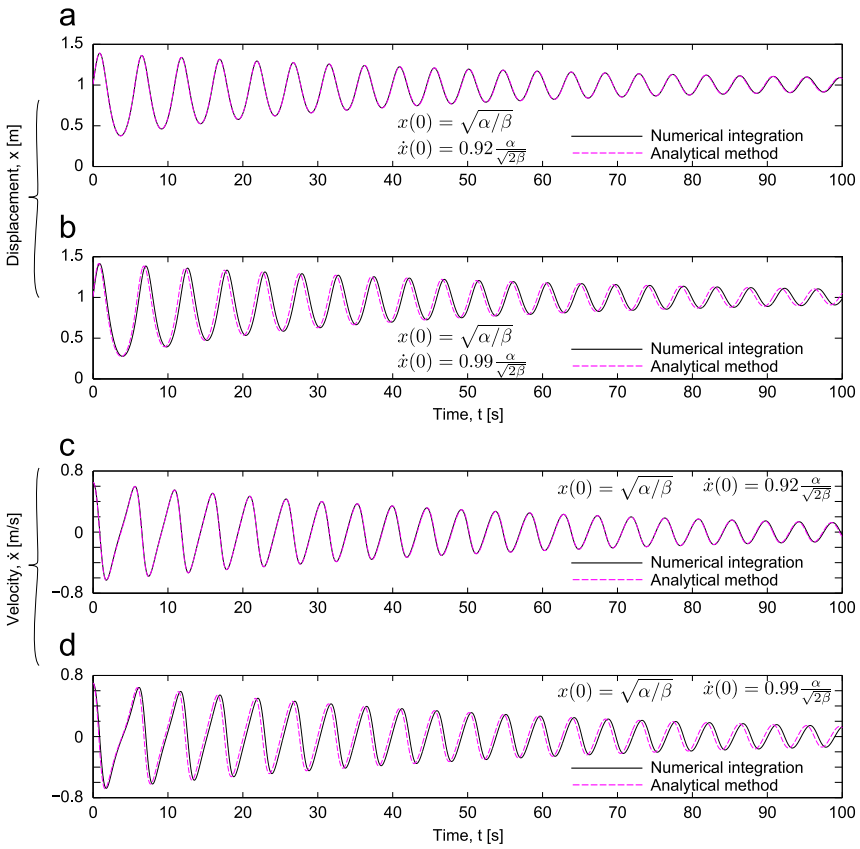

Fig. 2. Transient intrawell dynamics of the bistable oscillator for $x_0 = +\sqrt{\alpha/\beta}$. Displacement when (a) $\dot{x}_0 = 0.92 \cdot \alpha/\sqrt{2\beta}$ and (b) $\dot{x}_0 = 0.99 \cdot \alpha/\sqrt{2\beta}$. Velocity when (c) $\dot{x}_0 = 0.92 \cdot \alpha/\sqrt{2\beta}$ and (d) $\dot{x}_0 = 0.99 \cdot \alpha/\sqrt{2\beta}$.

oscillations. To satisfy the constraint $0.5 \le \alpha/\beta D_0^2 \le 1$ for intrawell vibration, the initial velocities considered for the intrawell behaviors satisfy $\dot{x}_0 \le \alpha/\sqrt{2\beta}$.

Fig. 2 illustrates two examples of (a,b) displacement and the corresponding (c,d) velocity trajectories for two initial velocities. Fig. 2(a) and (c) shows results for $\dot{x}_0 = 0.92 \cdot \alpha/\sqrt{2\beta}$; the results plotted in Fig. 2(b) and (d) are for $\dot{x}_0 = 0.99 \cdot \alpha/\sqrt{2\beta}$ which indicates the initial velocity is only 1% less than that required to activate interwell oscillations. In the figures, the dark/solid curves are the exact, numerically-integrated results, while the light/dashed curves are the analytical predictions. For the smaller initial velocity, the analytical predictions shown in Fig. 2(a) and (c) are in excellent agreement with the numerical findings. On the other hand, for the larger initial velocity, the instantaneous displacement and velocity phases exhibit greater deviation with respect to the numerical, exact results, Fig. 2(b) and (d). This is due to the reduced fidelity of the polynomial fit for the regimes $\alpha/\beta D_0^2$ near 0.5. Recalling Section 3.1, the fit was made across $0.55 \le \alpha/\beta D^2 \le 1$ with good success (very large R^2), although intrawell oscillations may also be obtained for $\alpha/\beta D^2$ as low as 0.5 (see Section 2.3). For the larger initial velocity condition of $\dot{x}_0 = 0.99 \cdot \alpha/\sqrt{2\beta}$, one finds that at the start of the transient oscillation prediction $\alpha/\beta D_0^2 = 0.5025$ which is outside of the polynomial fitting regime. Thus, the approximated form of the function $f\left(k_d^2\right)$ has reduced fidelity for the case having larger initial velocity, which is the source of the deviation between the numerical and analytical results shown in Fig. 2(b) and (d). On the other hand, the analytically-predicted time-varying amplitudes of displacement and velocity are still in excellent agreement in spite of the instantaneous deviation of phases with respect to the exact, numerical results.

The dissipative intrawell oscillations should ultimately settle to the stable equilibrium $x|_{t\to\infty} = x^* = +\sqrt{\alpha/\beta}$. Yet, due to the fitting limitations for one polynomial, a finite deviation exists between the fit at the extreme of the range where $\alpha/\beta D^2 = 1$ such that $D = +\sqrt{\alpha/\beta}$ when $t \to \infty$. In fact, according to the parameters used for the fit, after a long time of oscillation, the analytically predicted final displacement amplitude, Eq. (30), is found to be

$$\lim_{t\to\infty} D(t) = \left(-\frac{\mu}{\upsilon}\right)^{1/4} \cdot \sqrt{\frac{\alpha}{\beta}} \approx 1.005\sqrt{\frac{\alpha}{\beta}}. \tag{51}$$

In other words, the final displacement amplitude predicted by the analytical method (according to the current fit parameters λ, μ, υ) deviates from the exact value with a relative error near 0.5%, such that the dissipative dynamics continue to oscillate even after an infinite time elapses (albeit, oscillate with equal positive and negative values around the stable equilibrium). Fig. 3 illustrates this interesting result for the cases (a) $\dot{x}_0 = 0.92 \cdot \alpha/\sqrt{2\beta}$ and (b) $\dot{x}_0 = 0.99 \cdot \alpha/\sqrt{2\beta}$, also verifying that the relative errors remain small, ~0.5%. Since the focus of this analytical approach is on the transient dynamics – thus primarily on those motions which occur while the system dissipates considerable energy – the accuracy achieved for intrawell vibrations close to the initial time, as shown in Fig. 2, is of greater interest than the small, persistent intrawell oscillations occurring at large times.

For a quantitative evaluation of the analytical prediction accuracy for intrawell oscillations across a large range of system parameters, the correlation coefficients between the analytical and numerical results are shown in Fig. 4 for three different initial velocities $\dot{x}_0 =$ (a) $0.92\alpha/\sqrt{2\beta}$, (b) $0.955\alpha/\sqrt{2\beta}$, and (c) $0.99\alpha/\sqrt{2\beta}$. The damping factor γ is chosen from a logarithmically spaced range of 300 values spanning [0.007079, 0.1], while the nonlinearity β is chosen from a linearly spaced range of 320 values over the range $\left[\alpha/\beta D_0^2,\ 2\alpha/\beta D_0^2\right]$ to satisfy the constraint $0.5 \le \alpha/\beta D_0^2 \le 1$ according to the initial velocity considered, and thus the

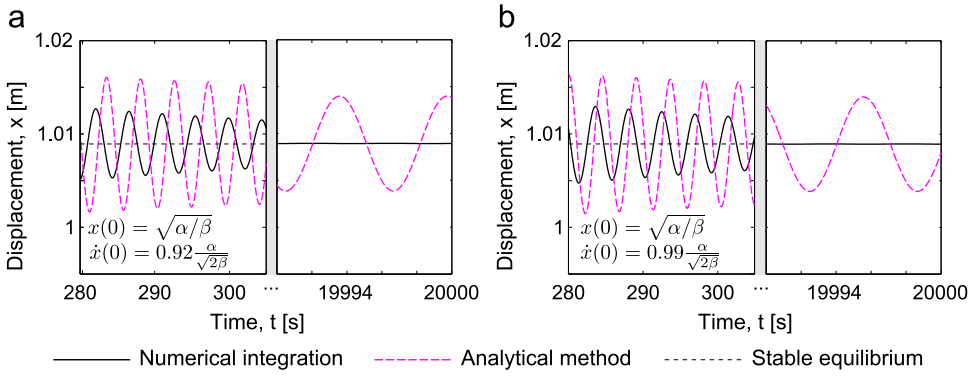

Fig. 3. Persistent intrawell oscillations at large times. $x_0 = +\sqrt{\alpha/\beta}$. Displacement when (a) $\dot{x}_0 = 0.92 \cdot \alpha/\sqrt{2\beta}$ and (b) $\dot{x}_0 = 0.99 \cdot \alpha/\sqrt{2\beta}$.

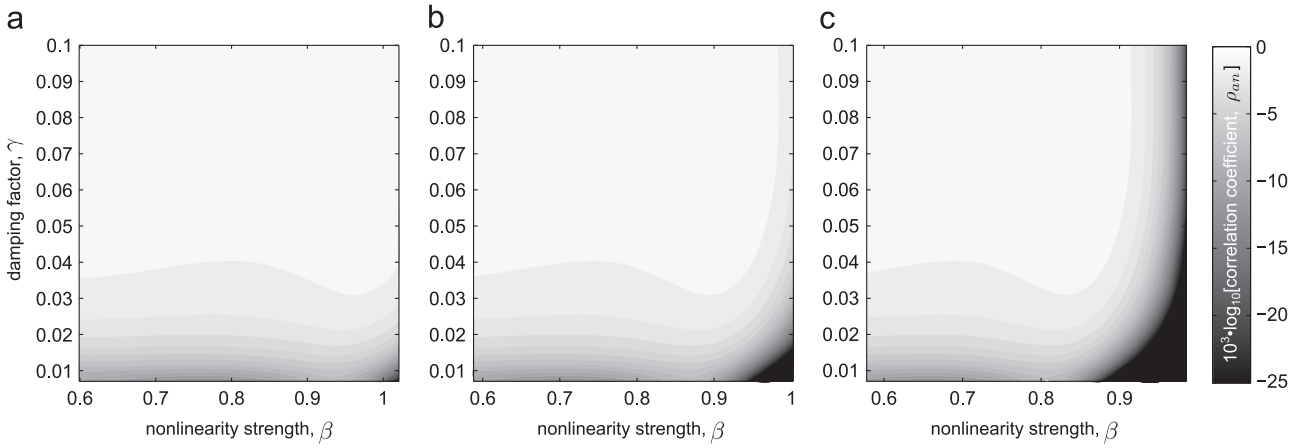

Fig. 4. Correlation coefficient between the numerical and analytical results of intrawell dynamics (using $10^3 \cdot \log_{10}(\rho_{a,n})$) with different initial velocities: $\dot{x}_0 =$ (a) $0.92\alpha/\sqrt{2\beta}$; (b) $0.955\alpha/\sqrt{2\beta}$ and (c) $0.99\alpha/\sqrt{2\beta}$. Lighter contour shadings indicate greater accuracy in the analytical prediction.

Table 1
Computation efficiency comparison for the intrawell vibration regime.

Initial velocity [m/s], $\dot{x}_0$	Computation time [min]		Analytical efficiency enhancement [%], $100 \cdot \frac{CT_n - CT_a}{CT_a}$
	Analytical, CT_a	Numerical, CT_n	
$0.92 \cdot \alpha/\sqrt{2\beta}$	**8.6090**	**45.4986**	**428**
$0.955 \cdot \alpha/\sqrt{2\beta}$	**8.5924**	**45.6261**	**431**
$0.99 \cdot \alpha/\sqrt{2\beta}$	**8.5717**	**57.4610**	**570**

initial displacement amplitude D_0 via Eq. (10). The correlation coefficient is computed over the time during which the difference in intrawell vibration amplitude from cycle-to-cycle is $\geqslant$0.1%. In effect, this takes the computation of $\rho_{a,n}$ out to very long times sufficient such that the instantaneous energy in the oscillators are negligible fractions of the initial input.

The results are plotted in Fig. 4, where the correlation coefficients are shaded in the contours using $10^3 \cdot \log_{10}(\rho_{a,n})$: dark shadings indicate large coefficient logarithms which indicates poor correlation and thus greater error between the analytical and exact numerical displacement trajectories. In other words, a shading value corresponding to $10^3 \cdot \log_{10}(\rho_{a,n}) = 0$ indicates perfect agreement (the lightest shading level employed in the figure). As seen in Fig. 4(a), when the initial velocity is only 8% less than that required to activate interwell oscillations ($\dot{x}_0 = 0.92\alpha/\sqrt{2\beta}$), the accuracy of the analytical prediction is very good for a significant range of the nonlinearity and damping parameters. For progressively increasing initial velocity, from Fig. 4(b) and (c), the fidelity of the analytical result reduces from the exact, numerically-integrated values, but primarily only for large nonlinearity strengths and smaller damping factors, as evidenced by the darker shading of the contours in those parameter regions. Yet, overall, for a substantial range of nonlinearity and damping parameters, the proposed analytical method yields exceptionally accurate results with respect to the exact intrawell dynamics, even when the initial velocity is only marginally smaller than that sufficient to activate interwell behaviors.

Taking another perspective, Table 1 presents the findings of the computation time required by the analytical and numerical approaches to reconstruct the intrawell trajectories, such that the results of Fig. 4 may be determined. The computations are carried out on a computer with 4 GB of RAM memory and a 3.00 GHz Intel Core 2 Duo processor. For these results, the evaluations for different damping factors γ and nonlinearity β parameters are over a grid 100 by 120, respectively, across the range of values shown in Fig. 4. Table 1 shows that the analytical approach enhances the computational efficiency of the large parametric evaluation of intrawell dynamic trajectories reconstruction, on average, by about 476%. In other words, to reconstruct to the transient intrawell dynamics to a high degree of accuracy (see Fig. 4), the analytical method developed herein provides a valuable computational efficiency improvement for those designing and operating structures which are bistable or buckled in such a way that the Duffing oscillator model is applicable.

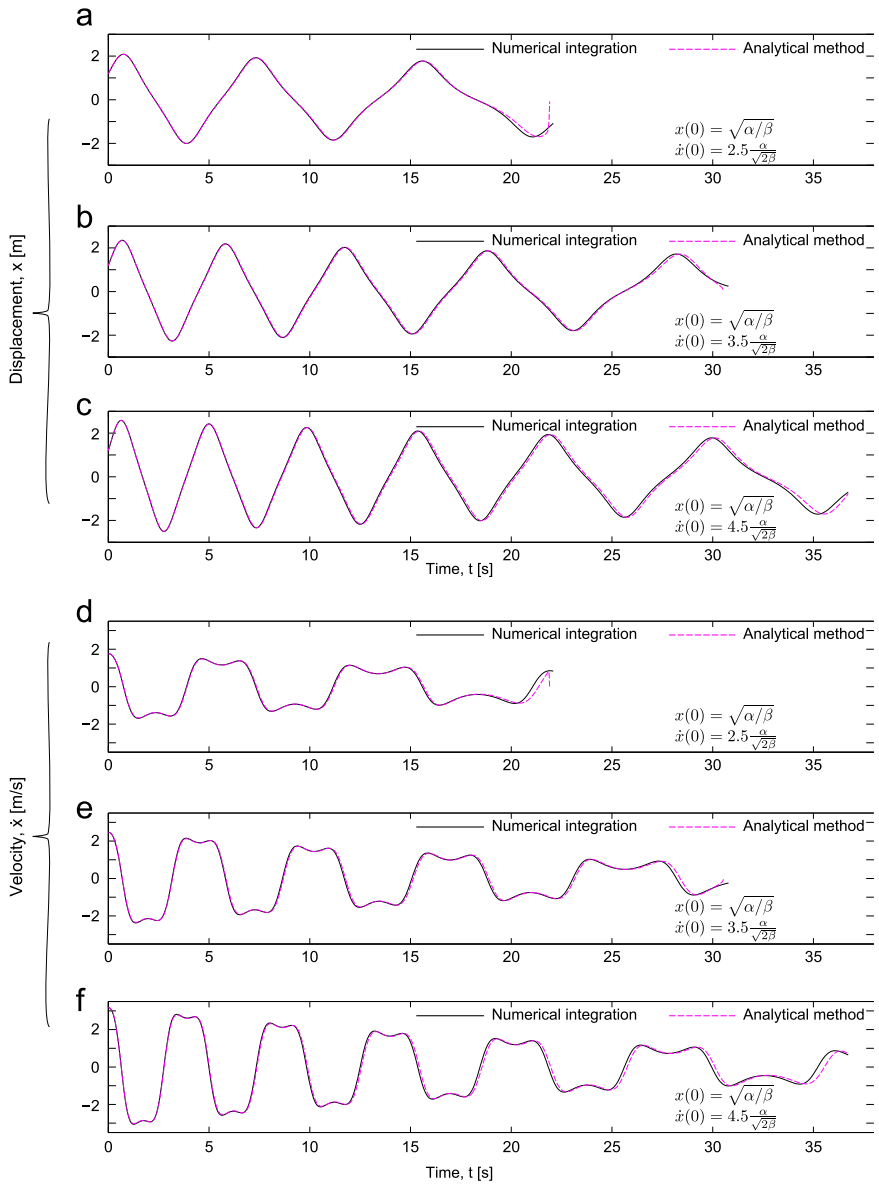

Fig. 5. Transient interwell dynamics of the bistable oscillator for $x_0 = +\sqrt{\alpha/\beta}$. Displacement when (a) $\dot{x}_0 = 2.5 \cdot \alpha/\sqrt{2\beta}$, (b) $\dot{x}_0 = 3.5 \cdot \alpha/\sqrt{2\beta}$, and (b) $\dot{x}_0 = 4.5 \cdot \alpha/\sqrt{2\beta}$. Velocity when (d) $\dot{x}_0 = 2.5 \cdot \alpha/\sqrt{2\beta}$, (e) $\dot{x}_0 = 3.5 \cdot \alpha/\sqrt{2\beta}$, and (f) $\dot{x}_0 = 4.5 \cdot \alpha/\sqrt{2\beta}$.

5.2. Transient interwell oscillations

Although intrawell dynamics may be predicted with high accuracy, the dissipative, interwell oscillations – which are far from equilibrium and indeed cross between both of them! – are historically challenging to analytically predict. To examine the accuracy of the proposed analytical method towards reconstructing the interwell dynamics, a first set of qualitative assessments is shown in Fig. 5 where the system parameters are $\gamma = 0.054317$ and $\beta = 0.70128$. Displacement predictions are shown in Fig. 5(a)–(c) while the corresponding velocity trajectories are given in Fig. 5 (d)–(f); the solid/dark curves indicate the numerical integration findings whereas light/dashed curves are the analytical predictions. The initial velocities are chosen such that $\dot{x}_0 \geq \alpha/\sqrt{2\beta}$ which is derived from Eq. (15) to satisfy the constraint for interwell vibration: $0 \leq \alpha/\beta C^2 \leq 0.5$. Fig. 5 provides examples for which the initial velocity $\dot{x}_0$ is (a,d) $2.5 \cdot \alpha/\sqrt{2\beta}$, (b,e) $3.5 \cdot \alpha/\sqrt{2\beta}$, and (c,f) $4.5 \cdot \alpha/\sqrt{2\beta}$ and plots out each pair of analytical and numerical predictions to the time at which the instantaneous energy of the respective result is $E(t) = 0$.

The examples in Fig. 5 demonstrate that the analytical predictions are in excellent qualitative agreement with the exact, numerical dynamics. A small degree of phase error is observed to accumulate over the prediction times which is more apparent for larger values of the initial velocity such as that in Fig. 5(c) and (f). An interesting feature is evident in Fig. 5(a) and (d) where the last analytically-predicted values of displacement and velocity, respectively, undergo a jump. Following close examination of such cases, it is seen that the integrand term $4\gamma\psi_c\left[\left(E_c/l_c^2\right) - K_c\right]$ for the elliptic function argument u_c in Eq. (50b) increases asymptotically at the final times of analytical prediction prior to $E(t) = 0$, where the rate of increase is dependent upon system parameters and the initial velocity. Since the argument u_c (i.e., instantaneous total phase) determines the output of the Jacobian elliptic function evaluation via Eq. (35), an argument which varies dramatically can induce a switch of sign between incremental evaluations of the elliptic function. The consequence is a potential for sudden deviation in value for the predicted displacement/velocity trajectories at the last sample of time prior to $E(t) = 0$. Although this feature is found to occur somewhat at random based upon the

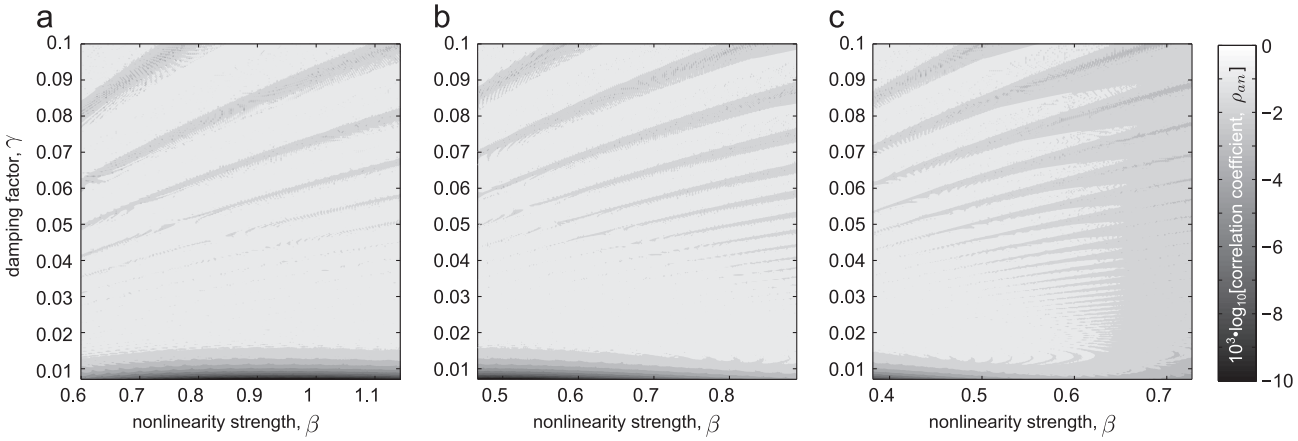

Fig. 6. Correlation coefficient between the numerical and analytical results of interwell dynamics (using $10^3 \cdot \log_{10}(\rho_{a,n})$) with different initial velocities: $\dot{x}_0 =$ (a) $2.5 \cdot \alpha/\sqrt{2\beta}$; (b) $3.5 \cdot \alpha/\sqrt{2\beta}$ and (c) $4.5 \cdot \alpha/\sqrt{2\beta}$. Lighter contour shadings indicate greater accuracy in the analytical prediction.

system parameters and initial velocity selections, it ultimately only influences the final displacement/velocity point predictions, and plays a small role as relates to the accuracy computed via the correlation coefficient.

A comprehensive assessment of the accuracy of the analytical method is given in Fig. 6 where a large range of nonlinearity and damping parameters are employed and the correlation coefficient, as $10^3 \cdot \log_{10}(\rho_{a,n})$, is plotted by the contour shading. To keep the computation consistent and meaningful, the correlation coefficient is taken between the numerical and analytical displacement data series from the initial time to the time that first results in $E(t) = 0$, whether this condition occurs numerically or by the analytical prediction. Three different initial velocities $\dot{x}_0$ are considered in Fig. 6, (a) $2.5 \cdot \alpha/\sqrt{2\beta}$, (b) $3.5 \cdot \alpha/\sqrt{2\beta}$, (c) and $4.5 \cdot \alpha/\sqrt{2\beta}$. The damping factor γ is chosen on the range of [0.007079, 0.1], while the nonlinearity strength β meets $\beta \geq 2\alpha/C_0^2$ to satisfy the constraint $0 \leq \alpha/\beta C^2 \leq 0.5$.

The results in Fig. 6 show that across this large span of system parameters a very high correlation coefficient (light shading of $10^3 \cdot \log_{10}(\rho_{a,n})$) is obtained which indicates high accuracy from the analytical predictions. Several trends are worth noting. First, a banded or striped feature is observed in the contours of Fig. 6. This is found to result from small changes in system parameters which induce one more or one less well-crossing event. Such cases show vulnerability in the analytical approach since these examples exhibit a significant slowing-down of dynamics prior to ultimately undergoing one more cross-well dynamic or returning to the local well of potential energy. On the other hand, the accuracy of analytical predictions is still very high as attested by the large correlation coefficients in the banded regions. Second, local, dark contour shadings are evident (almost dot-like) which indicate reductions in the prediction accuracy. These features result from the local parametric selections which induce the poor final time predictions and thus jump in the displacement trajectories, such as the example shown in Fig. 5(a) and elucidated above. Finally, for the results obtained using the larger initial velocity, Fig. 6(c), an increase in the error is shown via darker shading when the nonlinearity values β are larger, regardless of the damping factor. It is seen that this trend results from a small accumulation of phase error between the analytical predictions and numerical results since the larger initial velocities induce longer periods of interwell oscillation for the same system parameters. On the other hand, the examination of specific examples amongst these parameters reveal that the final amplitude and final time at which the interwell oscillations are predicted to occur do not significantly deviate from the exact, numerical values in spite of the phase error. Thus, for a large range of parameters and initial velocities, the analytical method also leads to exceptionally high accuracy of predictions for the interwell dynamics.

Table 2
Computation efficiency comparison for the interwell vibration dynamic regime.

Initial velocity [m/s], $\dot{x}_0$	Computation time [min]		Analytical efficiency enhancement [%], $100 \cdot \frac{CT_n - CT_a}{CT_a}$
	Analytical, CT_a	Numerical, CT_n	
$2.5 \cdot \alpha/\sqrt{2\beta}$	**8.2771**	**31.1330**	**276**
$3.5 \cdot \alpha/\sqrt{2\beta}$	**8.7314**	**37.2208**	**340**
$4.5 \cdot \alpha/\sqrt{2\beta}$	**9.0337**	**41.8872**	**364**

Table 2 presents the corresponding computational time and efficiency assessment results for the interwell dynamic regime evaluation shown in Fig. 6. By using the analytical method developed in this research, the data in Table 2 indicate that the computation time to obtain accurate transient dynamics reconstruction is reduced on average by more than a factor of 3: thus, the efficiency enhancement averages about 327%. These results suggest that for engineering applications, such as understanding the number of snap-through cycles that might occur for buckled and impulse-excited aircraft panels, able to be modeled using the bistable Duffing oscillator governing equation, the analytical method may greatly enhance the predictive capabilities of the engineer and designer via providing an accurate and computationally efficient trajectory reconstruction scheme.

6. Discussion

In this section, final remarks are provided to summarize the capabilities and limitations of the analytical prediction strategy developed in this research. First, although this investigation has examined the sensitivity of the analytical strategy using different initial velocities while the initial displacements have remained fixed, the authors note from a large variety of case studies not presented here that the strategy is found to be similarly accurate in predicting the transient dynamics for any combination of initial conditions. On the other hand, while providing high overall accuracy according to the correlation coefficient criterion, as observed in Figs. 2 and 5 the analytical reconstruction of trajectories may induce an accumulation of phase error for certain initial conditions. In practice, this may be unfavorable should one be interested in the instantaneous oscillator phase, for example to prescribe active controls to the bistable system. The planned,

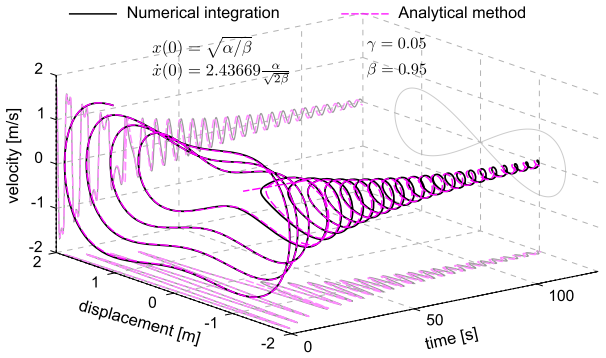

Fig. 7. Comparing the fully-reconstructed analytical prediction (light dashed curves) with the numerically-integrated, exact results (dark solid curves). The light solid curve on the far displacement–velocity plane is the homoclinic orbit.

future efforts of the authors include a comprehensive study on the role of initial conditions on the dynamical reconstruction accuracy.

Next, although good agreement is obtained for a vast range of system parameters of nonlinearity and damping in terms of predicting the dynamic response amplitudes $D(t)$ and $C(t)$ – which are derived in a purely analytical *closed-form*, see Eqs. (30) and (45) – the reconstruction of the instantaneous displacement and velocity trajectories necessitate a pseudo-analytical determination. This is because such trajectories rely on the time-varying amplitudes as well as on the time-varying arguments and moduli, the former which must be numerically evaluated, see Eqs. (34) and (50). On the other hand, as summarized via Tables 1 and 2, the analytical method leads to appreciable computational performance improvements when compared to direct numerical integration by a fourth-order Runge–Kutta algorithm. Thus, despite the pseudo-analytical nature of the transient displacement and velocity trajectories, the analytical prediction tools developed in this study are accurate as well as computationally efficient. Moreover, the designer or engineer that requires knowledge only of the dynamic regime time extents or the instantaneous response amplitude or frequency may take full advantage of the *closed-form* analytical approximations of these characteristics for expedited development and design iteration of systems that incorporate bistable or buckled components suitable to be modeled using the bistable Duffing oscillator governing equation of motion.

Finally, one may ask why the solution strategy developed here does not integrate the interwell and intrawell dynamics predictions when the initial velocity is great enough to induce cross-well behaviors. In other words, why does the strategy reconstruct the dynamics in pieces rather than continuously like that shown in Fig. 1(b)? In fact, several efforts to achieve this ideal were undertaken in this research, but none were fruitful. A number of challenges could be elucidated from such experiences, but a more meaningful justification for the difficulties may be given by a qualitative commentary. Consider that the transition from inter- to intrawell oscillations represents a bifurcation in the overall dynamics: the trajectory crosses the homoclinic orbit, see Fig. 1(b), and the global dynamical behavior of the oscillations change significantly. Under such conditions, the bifurcating dynamics occur on a time scale sufficiently slower than the natural periods of free decaying oscillation [12]. As a result, the effective mathematical treatment and reconstruction of such dynamics transition requires an assessment of the system when reduced to a more appropriate equation form, namely a normal form [34,35]. This is not to suggest that a unified prediction approach is impossible but rather that alternative methods may be needed to establish such a framework. Nevertheless, a direct splicing of inter- to intrawell dynamics predictions may be effected by using the final states determined for the interwell dynamics as the initial conditions for the intrawell prediction. It is seen that this strategy results in overall good agreement in many cases. For example, the example shown in Fig. 7 plots the corresponding analytical results with the numerical data previously presented in Fig. 1(b). Albeit imperfect, the agreement is nevertheless very good and represents a major step forward in the accurate prediction of such strongly nonlinear, transient dynamics.

7. Conclusion

This research developed a new and enhanced averaging method using the Jacobian elliptic functions to analytically reconstruct the transient, dissipative dynamics of a bistable Duffing oscillator. By relaxing the requirement for small variation of the averaged parameters as employed classically, the proposed analytical strategy enables an accurate, long-time prediction of the transient dynamics, whether of the intra- or interwell dynamic regimes. Comprehensive assessments find that the analytical predictions realize excellent agreement in the decaying amplitudes of oscillation when compared to the exact results determined by numerical integration. The instantaneous phase exhibits small deviation with respect to the exact results for some system parameters and initial conditions. The time-varying amplitudes of displacement and velocity are derived in an analytical closed-form, while the reconstruction of the corresponding instantaneous trajectories requires a pseudo-analytical approach that is found to be much more computationally efficient, for a high degree of accuracy, than a conventional numerical integration scheme. Overall, the considerable accuracy and efficiency of the proposed prediction method open the door to the implementation of the method in settings where such transient behaviors are of importance, including understanding the shock vulnerability in structural design and the effective development of bistable vibration-based energy harvesters under impulsive excitations.

Acknowledgments

This work is supported in part by the National Natural Science Foundation of China (No. 51475356), the Chinese Scholarship Council (CSC), and the University of Michigan Collegiate Professorship.

References

[1] L.N. Virgin, Vibration of Axially Loaded Structures, Cambridge University Press, Cambridge, 2007.
[2] J. Qiu, J.H. Lang, A.H. Slocum, A curved-beam bistable mechanism, J. Microelectromech. Syst. 13 (2004) 137–146.
[3] T.J. Kazmierski, S. Beeby, Energy Harvesting Systems: Principles, Modeling and Applications, Springer, New York, 2011.
[4] R.L. Harne, K.W. Wang, A review of the recent research on vibration energy harvesting via bistable systems, Smart Mater. Struct. 22 (2013) 023001.
[5] G. Debnath, T. Zhou, F. Moss, Remarks on stochastic resonance, Phys. Rev. A 39 (1989) 4323–4326.
[6] M.I. Dykman, A.L. Velikovich, G.P. Golubev, D.G. Luchinskiĭ, S.V. Tsuprikov, Stochastic resonance in an all-optical passive bistable system, Sov. Phys. JETP Lett. 53 (1991) 193–197.
[7] N. Hu, R. Burgueño, Buckling-induced smart applications: recent advances and trends, Smart Mater. Struct. 24 (2015) 063001.
[8] Michelin. Michelin Tweel. [Online]. ⟨http://www.michelintweel.com/⟩, 2015.
[9] J.S. Humphreys, On dynamic snap buckling of shallow arches, AIAA J. 4 (1966) 878–886.
[10] A.N. Kounadis, J. Raftoyiannis, J. Mallis, Dynamic buckling of an arch model under impact loading, J. Sound Vib. 134 (1989) 193–202.
[11] M.I. Dykman, D.G. Luchinsky, R. Mannella, P.V.E. McClintock, N.D. Stein, N. G. Stocks, Stochastic resonance in perspective, IL Nuovo Cimento 17 (1995) 661–683.

[12] R. Seydel, Practical Bifurcation and Stability Analysis, Springer, New York, 2010.
[13] R.E. Mickens, A generalization of the method of harmonic balance, J. Sound Vib. 111 (1986) 515–518.
[14] S.B. Yuste, J.D. Bejarano, Improvement of a Krylov–Bogoliubov method that uses Jacobi elliptic functions, J. Sound Vib. 139 (1990) 151–163.
[15] I. Kovacic, M.J. Brennan, The Duffing Equation: Nonlinear Oscillators and Their Behaviour, John Wiley & Sons, Chichester, 2011.
[16] P.G.D. Barkham, A.C. Soudack, An extension to the method of Kryloff and Bogoliuboff, Int. J. Control 10 (1969) 377–392.
[17] M. Belhaq, F. Lakrad, The elliptic multiple scales method for a class of autonomous strongly non-linear oscillators, J. Sound Vib. 234 (2000) 547–553.
[18] A.C. Soudack, P.G.D. Barkham, On the transient solution of the unforced Duffing equation with large damping, Int. J. Control 13 (1971) 767–770.
[19] P.G.D. Barkham, A.C. Soudack, Approximate solutions of non-linear non-autonomous second-order differential equations, Int. J. Control 11 (1970) 101–114.
[20] P.A.T. Christopher, A. Brocklehurst, A generalized form of an approximate solution to a strongly non-linear, second-order, differential equation, Int. J. Control 19 (1974) 831–839.
[21] R.E. Mickens, Truly Nonlinear Oscillators: Harmonic Balance, Parameter Expansions, Iteration, and Averaging Methods, World Scientific, London, 2010.
[22] S.B. Yuste, Comments on the method of harmonic balance in which Jacobi elliptic functions are used, J. Sound Vib. 145 (1991) 381–390.
[23] L. Cveticanin, Homotopy-perturbation method for pure nonlinear differential equation, Chaos Solitons Fractals 30 (2006) 1221–1230.
[24] J.H. He, Comparison of homotopy perturbation method and homotopy analysis method, Appl. Math. Comput. 156 (2004) 527–539.
[25] F. Lakrad, M. Belhaq, Periodic solutions of strongly non-linear oscillators by the multiple scales method, J. Sound Vib. 258 (2002) 677–700.
[26] S.B. Yuste, "Cubication" of non-linear oscillators using the principle of harmonic balance, Int. J. Non-Linear Mech. 27 (1992) 347–356.
[27] L. Cveticanin, An approximate solution for a system of two coupled differential equations, J. Sound Vib. 152 (1992) 375–380.
[28] V.T. Coppola, R.H. Rand, Averaging using elliptic functions: approximation of limit cycles, Acta Mech. 81 (1990) 125–142.
[29] V.T. Coppola, R.H. Rand, Macsyma program to implement averaging using elliptic functions, in: K.R. Meyer, D.S. Schmidt (Eds.), Computer Aided Proofs in Analysis, Springer, New York, 1991, pp. 71–89.
[30] M. Belhaq, F. Lakrad, Prediction of homoclinic bifurcation: the elliptic averaging method, Chaos Solitons Fractals 11 (2000) 2251–2258.
[31] M.A. Al-Shudeifat, Amplitudes decay in different kinds of nonlinear oscillators, J. Vib. Acoust. 137 (2015) 031012.
[32] T. Okabe, T. Kondou, J. Ohnishi, Elliptic averaging methods using the sum of Jacobian elliptic delta and zeta functions as the generating solution, Int. J. Non-Linear Mech. 46 (2011) 159–169.
[33] P.F. Byrd, M.D. Friedman, Handbook of Elliptic Integrals for Engineers and Scientists, Springer-Verlag, Berlin, Heidelberg, New York, 1971.
[34] J. Guckenheimer, P.J. Holmes, Nonlinear Oscillations, Dynamical Systems, and Bifurcations of Vector Fields, Springer, New York, 1983.
[35] Y.A. Kuznetsov, Elements of Applied Bifurcation Theory, Springer, New York, 1998.